Uncovering the geometry of the hot X-ray corona in the Seyfert galaxy NGC 4151 with IXPE

V. E. Gianolli,[1,2]★ D. E. Kim,[3,4,5]† S. Bianchi,[2] B. Agís-González,[6] G. Madejski,[7] F. Marin,[8] A. Marinucci,[9] G. Matt,[2] R. Middei,[3,10] P-O. Petrucci,[1] P. Soffitta,[3] D. Tagliacozzo,[2] F. Tombesi,[5,11,12] F. Ursini,[2] T. Barnouin,[8] A. De Rosa,[3] L. Di Gesu,[9] A. Ingram,[13] V. Loktev,[14] C. Panagiotou,[15] J. Podgorny,[8,16,17] J. Poutanen,[14] S. Puccetti,[10] A. Ratheesh,[3] A. Veledina,[14,18] W. Zhang,[19] I. Agudo,[6] L. A. Antonelli,[10,20] M. Bachetti,[21] L. Baldini,[22,23] W. H. Baumgartner,[24] R. Bellazzini,[22] S. D. Bongiorno,[24] R. Bonino,[25,26] A. Brez,[22] N. Bucciantini,[27,28,29] F. Capitanio,[3] S. Castellano,[22] E. Cavazzuti,[9] C.-T. Chen ,[30] S. Ciprini,[10,11] E. Costa,[3] E. Del Monte,[3] N. Di Lalla,[7] A. Di Marco,[3] I. Donnarumma,[9] V. Doroshenko,[31] M. Dovčiak,[16] S. R. Ehlert,[24] T. Enoto,[32] Y. Evangelista,[3] S. Fabiani,[3] R. Ferrazzoli,[3] J. A. García,[33] S. Gunji,[34] J. Heyl,[35] W. Iwakiri,[36] S. G. Jorstad,[37,38] P. Kaaret,[24] V. Karas,[16] F. Kislat,[39] T. Kitaguchi,[32] J. J. Kolodziejczak,[24] H. Krawczynski,[40] F. La Monaca,[3] L. Latronico,[25] I. Liodakis,[41] S. Maldera,[25] A. Manfreda,[22] A. P. Marscher,[37] H. L. Marshall,[15] F. Massaro,[25,26] I. Mitsuishi,[42] T. Mizuno,[43] F. Muleri,[3] M. Negro,[44,45,46] C.-Y. Ng,[47] S. L. O'Dell,[24] N. Omodei,[7] C. Oppedisano,[25] A. Papitto,[20] G. G. Pavlov,[48] A. L. Peirson,[7] M. Perri,[10,20] M. Pesce-Rollins,[22] M. Pilia,[21] A. Possenti,[21] B. D. Ramsey,[24] J. Rankin,[3] O. J. Roberts,[30] R. W. Romani,[7] C. Sgrò,[22] P. Slane,[49] G. Spandre,[22] D. A. Swartz ,[30] T. Tamagawa,[32] F. Tavecchio,[50] R. Taverna,[51] Y. Tawara,[42] A. F. Tennant,[24] N. E. Thomas,[24] A. Trois,[21] S. S. Tsygankov,[14] R. Turolla,[51,52] J. Vink,[53] M. C. Weisskopf,[24] K. Wu,[52] F. Xie,[54,3] and S. Zane[52]

Affiliations are shown at the end of the paper

Accepted XXX. Received YYY; in original form ZZZ

ABSTRACT

We present an X-ray spectro-polarimetric analysis of the bright Seyfert galaxy NGC 4151. The source has been observed with the *Imaging X-ray Polarimetry Explorer* (*IXPE*) for 700 ks, complemented with simultaneous *XMM-Newton* (50 ks) and *NuSTAR* (100 ks) pointings. A polarization degree $\Pi = 4.9 \pm 1.1\%$ and angle $\Psi = 86° \pm 7°$ east of north (68% confidence level) are measured in the 2–8 keV energy range. The spectro-polarimetric analysis shows that the polarization could be entirely due to reflection. Given the low reflection flux in the *IXPE* band, this requires however a reflection with a very large ($> 38\%$) polarization degree. Assuming more reasonable values, a polarization degree of the hot corona ranging from ~ 4 to $\sim 8\%$ is found. The observed polarization degree excludes a 'spherical' lamppost geometry for the corona, suggesting instead a *slab*-like geometry, possibly a *wedge*, as determined via Monte Carlo simulations. This is further confirmed by the X-ray polarization angle, which coincides with the direction of the extended radio emission in this source, supposed to match the disc axis. NGC 4151 is the first AGN with an X-ray polarization measure for the corona, illustrating the capabilities of X-ray polarimetry and *IXPE* in unveiling its geometry.

Key words: galaxies: active – galaxies: Seyfert – galaxies: individual: NGC 4151 – polarization

1 INTRODUCTION

The common paradigm for Active Galactic Nuclei (AGN) (Antonucci 1993) postulates the presence of a corona of hot electrons ($kT_e \simeq 10$–100 keV), responsible for the primary continuum in the hard X-rays through Inverse Comptonization of UV photons (Sunyaev &

★ E-mail: vittoria.gianolli@univ-grenoble-alpes.fr
† E-mail: dawoon.kim@inaf.it

Titarchuk 1980; Zdziarski et al. 2000). Despite widespread acceptance of this process, the source of energy for the plasma and the conditions leading to its formation remain open questions. The geometry of this region further contributes to these debates, ranging from a *slab*-corona model (Haardt & Maraschi 1991, 1993; Merloni 2003), in which the energy dissipation and electron heating occur over a large volume, to a possible aborted jet located on the accretion disc axis (lamppost geometry; see Ghisellini et al. 2004; Fabian et al. 2017). Compton scattering will produce a polarization signal which is strongly sensitive to the geometry of the scattering material. Although spectroscopy and timing alone were not been able to distinguish between geometrical models so far, their application alongside polarization can aid in determining the characteristics of the corona such as the Thomson optical depth τ and the electron temperature kT_e (Shapiro et al. 1976). X-ray polarimetry is thus a powerful tool that can be used to bring new insights on the innermost regions of AGN. In particular, from 'spherical' lamppost coronae, a polarization degree of one percent or so is expected, while larger values are anticipated when the scattering medium is distributed as a *slab* over the accretion disc (Poutanen & Svensson 1996; Tamborra et al. 2018; Ursini et al. 2022).

The Imaging X-ray Polarimetry Explorer (*IXPE*, Weisskopf et al. 2022), launched on December 9, 2021, is a NASA/ASI mission and the first X-ray imaging polarimeter in orbit after 40 years. Thanks to three telescopes with polarization-sensitive imaging detectors (gas-pixel detector, Costa et al. 2001) effective in the 2–8 keV energy band, X-ray polarimetric studies on AGN are being carried out for the first time. So far a total of four radio-quiet AGN (i.e., MCG-05-23-16, the Circinus galaxy, NGC 4151 and IC 4329A) have been observed by *IXPE*. A polarization degree $\Pi < 4.7\%$ was derived for MCG-05-23-16, in agreement with expectations from a lamppost 'spherical' geometry of the corona, or a *slab* geometry if the inclination angle of the system is less than 50° (Marinucci et al. 2022). On the other hand, the Circinus galaxy shows a very high $\Pi \sim 28 \pm 7$ % with a polarization angle perpendicular to the radio jet at about $\psi_X \sim 18 \pm 5°$ (Ursini et al. 2023). However, this source is Compton-thick with no direct view of the corona, so all the polarization is ascribed to reflection from an equatorial torus, as expected from the standard Unification Model.

NGC 4151 is one of the brightest Seyfert galaxies in the local universe. It has been classified as a Changing Look AGN (Penston & Perez 1984; Puccetti et al. 2007; Shapovalova et al. 2008), going from optical type 1.5 at high flux states (in which the source reaches up to $F_{0.5-10\,\mathrm{keV}} \sim 2.8\times 10^{-10}$ erg s^{-1} cm^{-2}) to optical type 1.8 at low fluxes states ($F_{0.5-10\,\mathrm{keV}} \sim 8.7\times 10^{-11}$ erg s^{-1} cm^{-2}; see Antonucci & Cohen 1983; Shapovalova et al. 2012; Beuchert et al. 2017a). NGC 4151 has been intensively observed by all major X-ray satellites. It is characterised with significant spectral variability, and a complex absorption structure, both from neutral and ionised gas (e.g. Beuchert et al. 2017a). Below ~2 keV, the soft X-ray emission is dominated by emission lines (e.g. Schurch et al. 2004), likely arising from photoionizated gas in the narrow-line region, as commonly found in obscured AGN (Bianchi et al. 2006; Guainazzi & Bianchi 2007; Bianchi et al. 2019). Previous studies found evidence for relativistic reflection off the accretion disc, suggesting a near-maximal spinning black hole (Cackett et al. 2014; Keck et al. 2015a; Beuchert et al. 2017a). Given a black hole (BH) mass of $4.57\times 10^7 M_\odot$ (from optical and UV reverberation, Bentz et al. 2006), the source has a relatively low Eddington ratio, 1% (Keck et al. 2015a).

In the following, we present the spectral and spectro-polarimetric analysis of the combined data from *IXPE*, *XMM-Newton* and *NuSTAR*, providing the most complete view to date of the inner accretion flow in NGC 4151. The paper is organized as follows. In Sect. 2, we describe the *IXPE*, *XMM-Newton* and *NuSTAR* observations and data reduction. In Sect. 3, we report on the spectral and spectro-polarimetric analysis. In Sect. 4 the results are discussed.

2 OBSERVATIONS AND DATA REDUCTION

IXPE (Weisskopf et al. 2022) observed NGC 4151 starting on December 8, 2022 with its three Detector Units (DU), for a net exposure time of about 632 ks. The data were calibrated with a standard *IXPE* pipeline from the Science Operation Center (SOC).[1] The pipeline mainly contains the correction processes on the photoionization events and the track reconstruction process following a standard moments analysis (Bellazzini et al. 2003; Fabiani & Muleri 2014; Di Marco et al. 2022). In addition, variations on gain properties that are caused by susceptibility of gas status (e.g., temperature and pressure) inside Gas Pixel Detector (GPD, Costa et al. 2001; Bellazzini et al. 2007; Fabiani et al. 2012; Baldini et al. 2021) and non-uniformity of the charging on the Gas Electron Multiplier (GEM) material are accounted for. The onboard calibration data was utilized to deal with the small time scale variations (Ferrazzoli et al. 2020). The spurious modulation was also taken into account in this process (Rankin et al. 2022). The scientific analysis was performed using the IXPEOBSSIM software version 30.2.1 (Baldini et al. 2022). Source and background data were extracted centered on the source position in the detector frame which covered the entire source emission and source-free regions respectively. For the region selection criteria, we applied a 72″ circle for the source and an annulus with an inner and outer radius of 150″ and 240″ for the background (Di Marco et al. 2023). In order to estimate the polarization properties, we created (1) the polarization cube (`PCUBE`) based on the Kislat et al. (2015) method, which provided results independent of any spectral modelling, and (2) I, Q, and U spectra using PHA1, PHAQ1, and PHAU1 algorithm in the `xpbin` tool inside IXPEOBSSIM. We utilised the version 12 instrument response functions for both methods, which are contained in IXPEOBSSIM. We adopted a minimum of 30 counts binning for spectra I and 0.2 keV constant energy binning for Q and U spectra in order to perform spectro-polarimetric analysis based on χ^2 statistics. For the spectra, we employed the weighted method (Di Marco et al. 2022) using the `alpha075` response matrix to improve the sensitivity of polarimetry measurements. In contrast, this feature is not currently available within the `pcube` algorithm.

XMM-Newton observed NGC 4151 on December 17, 2022 for 50 ks of elapsed time with the EPIC pn (Strüder et al. 2001) and the two MOS (Turner et al. 2001) cameras, operating in Small Window and thin filter mode to avoid pile-up effects. Background flares were present during the observation and after the filtering process, the effective exposure time resulted to be of about 33 ks for the pn spectrum. The extraction radii for the source and the background spectra are 20″ and 30″, respectively. The effective area was corrected with the new SAS keyword, APPLYABSFLUXCORR, expressly implemented to provide a better agreement with simultaneous *NuSTAR* data.

The *NuSTAR* (Harrison et al. 2013) observation started on December 16, 2022 simultaneously to *XMM* and *IXPE* pointings, with both coaligned X-ray telescopes with Focal Plane Module A (FPMA) and B (FPMB). The `Nupipeline` task and the latest calibration files available in the database (CALDB 20221229) were used to produce and

[1] https://heasarc.gsfc.nasa.gov/docs/ixpe/analysis/IXPE-SOC-DOC-009-UserGuide-Software.pdf

Table 1. Polarization parameters for different energy bands.

Energy range (keV)	$\Pi_X \pm 1\sigma$ (%)	$\psi_X \pm 1\sigma$ (deg)
2.0 – 8.0	4.9 ± 1.1	86 ± 7
2.0 – 3.5	4.3 ± 1.6	42 ± 11
3.5 – 5.0	5.0 ± 1.4	99 ± 8
5.0 – 8.0	7.4 ± 1.9	88 ± 7

calibrate cleaned event files. In this case the source and background extraction radii are 2′ and 1.22′, respectively. The net exposure time for the FPMA and FPMB resulted to be 97 ks and 96.3 ks. Significant deviations from the pn spectrum were still present in the *NuSTAR* spectra below 4 keV, even after applying the correction mentioned above. Therefore, we will consider *NuSTAR* data only above 4 keV (see e.g. Madsen et al. 2020). Moreover, an energy shift between the two instruments is evident at the iron line.[2] In the following fits, we thus applied a linear GAIN FIT of ∼ 60 eV to the *NuSTAR* spectra. We note here that a similar shift is found in AGN observations taken ∼1 month before and after our dataset (Serafinelli et al., in prep.; Ingram et al., in prep.).

All the uncertainties are given at 68% (1σ) confidence level, unless otherwise stated, while the upper/lower limits are quoted at 99% (2.6σ) confidence level for one interesting parameter. Throughout our analysis, we adopt a redshift $z = 0.003326$ for NGC 4151 (Wolfinger et al. 2013), and the cosmological parameters $H_0 = 70\,\mathrm{km\,s^{-1}\,Mpc^{-1}}$, $\Lambda_0 = 0.73$ and $\Lambda_m = 0.27$.

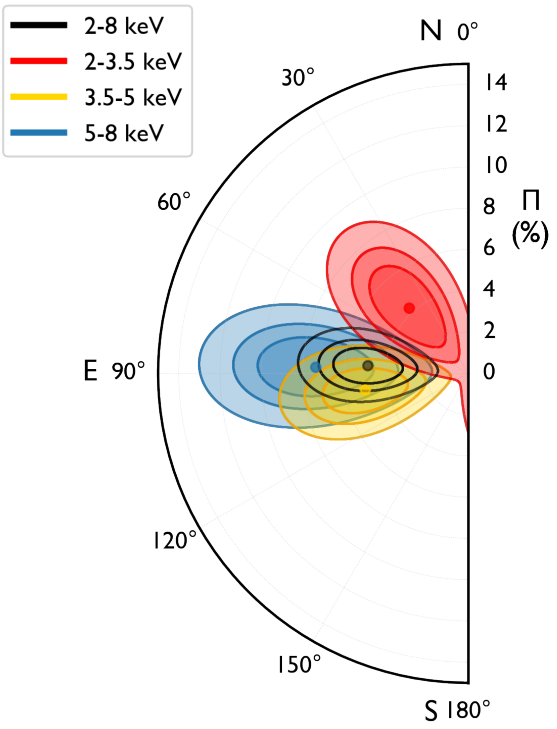

Figure 1. Polarization contours (68%, 90%, and 99% confidence levels for two degrees of freedom) for the polarization degree Π_X and the polarization angle ψ_X with respect to the north direction. Colors refer to the 2.0–8.0 keV (black), 2.0–3.5 keV (red), 3.5–5.0 keV (yellow), and 5.0–8.0 keV (blue) energy ranges, respectively.

3 DATA ANALYSIS

3.1 *IXPE* polarimetric analysis

We report the first significant polarization detection from NGC 4151 using PCUBE analysis. The measured polarization parameters from the three combined DUs are $\Pi_X = 4.9\% \pm 1.1\%$ and $\psi_X = 86° \pm 7°$ in the 2–8 keV band with background subtraction. The detection significance of these polarization properties is above 99.99% confidence level (∼ 4.4σ). In order to examine the energy dependency of the polarization, we tested against the hypothesis that Q and U Stokes parameters are constant via a χ^2 test, adopting different energy binnings (from 2 to 12 bins over the entire energy band, e.g. Di Gesu et al. 2022). We found a statistically significant (> 99% confidence level) deviation from the constant behaviour in Q, when adopting three and four bins. Figure 1 and Table 1 show the data into 3 energy bands: 2.0–3.5, 3.5–5.0, and 5.0–8.0 keV. In the polarization contour plot, significant detections are found for the two higher-energy bins (3.5–5.0 and 5.0–8.0 keV), while only a marginal detection can be claimed for the first bin (2.0–3.5 keV), possibly suggesting also a variation of the polarization angle, thus confirming the variability in Q mentioned above.

3.2 Spectral Analysis: *XMM-Newton* and *NuSTAR*

The spectral analysis of NGC 4151 is performed with XSPEC 12.13.0 (Arnaud 1996), taking into account the simultaneous 0.5–10 keV *XMM-Newton* and 4–79 keV *NuSTAR* spectra. In the new observations, the source has been detected in a high flux state with $F_{0.5-10\,\mathrm{keV}} \sim 1.7\times 10^{-10}$ erg s^{-1} cm^{-2}.

As mentioned in Sect. 1, the X-ray spectrum of this source is remarkably complex with different emission and absorption components (e.g., Weaver et al. 1994; Zdziarski et al. 1996; Yang et al. 2001; De Rosa et al. 2007; Kraemer et al. 2008; Lubiński et al. 2010). Our best fit model implements and tries to simplify those adopted by Keck et al. (2015a) and Szanecki et al. (2021) for the previous *XMM-Newton*, *Suzaku* and *NuSTAR* observations of the source. The Galactic absorbing column density, modelled with `tbabs`, is set to $N_H = 2.3 \times 10^{20}$ cm^{-2} (Kalberla et al. 2005) and multiplicative constants (found to be of the order of ∼ 1.20) take into account cross-calibration uncertainties between the two FPM modules and EPIC pn, as well as some flux variability of the source during the longer elapsed time of the *NuSTAR* observation. We adopt the default abundance table in XSPEC (Anders & Grevesse 1989).

In previous studies, a strong Fe Kα emission line with a weak relativistic component was reported in high flux states (e.g. Zoghbi et al. 2019). In the new *XMM-Newton* and *NuSTAR* observations, the Fe Kα line profile clearly shows the imprints of significant ionized absorption, which contributes to produce an overall modest redshift in energy. However, no indications of further broader components are found, the line being well modelled by a single Gaussian with a resolved width of $\sigma = 40 \pm 10$ eV and an equivalent width of EW = 100 ± 6 eV. Therefore in the following, also to simplify the spectro-polarimetric fit presented in Sect. 3.3, we will not include any relativistic reflection component in our model, as instead used in Keck et al. (2015a) and Szanecki et al. (2021). In any case, we

[2] The shift is still present if strictly simultaneous *NuSTAR–XMM* spectra are considered. On the other hand, the MOS data are in perfect agreement with the pn.

note here that we verified that including a relativistic reflection component to our broadband model gives a similar fit, not affecting in a significant way the other main parameters of the model.

We model the primary continuum with a thermally Comptonized continuum (`nthcomp` in XSPEC, Zdziarski et al. 1996; Życki et al. 1999), assuming seed photons from a disc-blackbody with temperature fixed at $kT_{\rm bb} = 8$ eV (as expected from a standard accretion disc with the BH mass and observed luminosity of NGC 4151, Shakura & Sunyaev 1973). For the reflection component, we used `BORUS` (Baloković et al. 2018, 2019), which models reprocessing from a torus with variable covering factor, self-consistently illuminated by a `nthcomp` spectrum with the same photon index and electron temperature as the primary continuum. In view of the joint spectro-polarimetric fit with the *IXPE* data presented in Sect. 3.3, we separated the reflection component from the corresponding fluorescent lines with the two dedicated `BORUS` tables, linking all the parameters (including the normalization). Since they are not constrained by the fit, we fixed the cosine of the inclination and the covering factor of the torus to 0.6 (appropriate for an intermediate Seyfert galaxy) and 0.5 (a standard value, e.g. Brightman et al. 2015; LaMassa et al. 2019), respectively. Moreover, in order to account for the modest broadening and redshift of the iron line as reported above, we convolve the `BORUS` tables with a `gsmooth` of $\sim$ 40 eV and a `vashift`[3] of the order of 1000 km s^{-1}.

The X-ray spectrum of NGC 4151 is well-known to be strongly affected by complex absorption. Similarly to Keck et al. (2015a), we used two partial-covering neutral absorbing layers (PC, modelled by `zpcfabs`) and a warm absorber (WA, modelled with `zxipcf` and covering factor fixed at 1). Finally, as suggested by the presence of emission lines at ~0.5 and ~ 0.9 keV and by previous results based on high-resolution spectra (Schurch et al. 2004; Guainazzi & Bianchi 2007; Bianchi et al. 2019), the remaining soft X-ray emission is modelled with a photoionized plasma emission component, produced with CLOUDY (Ferland et al. 1998) closely to what described in Bianchi et al. (2010). Some further residuals due to an imperfect modelization of the photoionized gas around the O VII emission line triplet at $\sim$ 0.5 keV are modelled with a Gaussian component.

In summary, our model can be written in XSPEC as `(tbabs)*(CLOUDY + zgauss + PC*PC*WA*(vashift*gsmooth*(BORUS 1 + BORUS 2) + nthcomp))`. This gives a good representation of the *XMM-Newton* + *NuSTAR* data with χ^2/d.o.f = 743/660.

The best fit parameters are reported in Table 2, while spectra and residuals are shown in Fig. 2. It is important to note that in this model the contribution of the reflection component to the total 2–8 keV flux is of the order of 6 per cent, reaching up to $\sim$ 16 per cent in the 6–8 keV band, due to the presence of the Fe Kα line. In the 2–3.5 keV band, no contribution from the photoionized emission is present, since it becomes significant only at lower energies (see Fig. 2). On the other hand, in this band there is an excess with respect to the absorbed primary continuum, which our model treats as the leakage of the primary emission through the partial coverers. Any other component, used to model this excess, would contribute up to 20 per cent of the total flux in the 2–3.5 keV band.

3.3 Spectro-polarimetric analysis: *XMM-Newton*, *NuSTAR* and *IXPE*

We added the *IXPE* data (I, Q and U spectra of the three detectors) to the *XMM-Newton*+*NuSTAR* best fit presented above, with all the spectral parameters linked to the other instruments, allowing only an inter-calibration constant (found to be of the order of $\sim$ 0.80) for each detector to vary. We then add separate `polconst` multiplicative models to account for the polarization of each additive component of the global model. The polarization degree Π and angle Ψ are set to 0 for the `BORUS` component producing the emission lines, since they are expected to be intrinsically not polarized, as well as for the CLOUDY component, which does not contribute at all in the *IXPE* energy band (see previous Section). On the other hand, the primary Comptonized continuum and the reflection component associated to the other `BORUS` table have Π and Ψ free to vary. The best fit gives χ^2/d.o.f= 1433/1264, with no appreciable variations in the spectral parameters with respect to the one without *IXPE*, being indeed dominated by the much higher sensitivity, spectral resolution and broad band coverage of *XMM-Newton* and *NuSTAR*. Considering the complex X-ray spectrum of NGC 4151 with multiple components in absorption and emission, the cross-calibration uncertainties among the several different instruments used, the variability of the source and the much longer exposure time of *IXPE* with respect to *XMM-Newton* and *NuSTAR*, we find this fit, if not ideal, acceptable given the goal of the paper. Moreover, we note that the fit applied only to the *IXPE* data gives a significantly better fit (χ^2/d.o.f= 672/612), confirming that the model is a good representation of the data in the 2-8 keV band, where all the polarimetric information is present.

In this configuration, we get loose constraints for the polarimetric parameters, i.e. $\Pi < 5\%$ and unconstrained angle for the primary continuum, and $\Pi > 38\%$ and $\Psi = 96^\circ \pm 16^\circ$ for the reflection component. We thus linked the angles of the two components, either to be equal or to differ by 90°. In both cases, we still obtain that the polarization is dominated by the reflection component, and the polarization degree of the primary emission is an upper limit. We therefore fixed the polarization properties of the reflection component to physically motivated values, 15, 20, 30 per cent (as found, for example, for the reflection-dominated Circinus galaxy, Ursini et al. 2023), constraining its polarization angle to be at 90° with respect to that of the primary emission. The resulting fits are marginally worse than the best fit, the χ^2 being 1452, 1453 and 1455 for 1266 d.o.f., respectively, and the polarization degree of the primary continuum is now constrained at $\Pi = 4.1 \pm 0.8\%$, $\Pi = 4.3 \pm 0.8\%$ and $\Pi = 4.6 \pm 0.8\%$ with polarization angles $\Psi = 82^\circ \pm 7^\circ$, $\Psi = 81^\circ \pm 7^\circ$ and $\Psi = 80^\circ \pm 8^\circ$, respectively.

These results may be driven by the lower Π and different Ψ observed in the 2–3.5 keV band (see Table 1), possibly due to another spectral component which dilutes the polarization of the primary continuum. We therefore modified the best fit model with a spectroscopically equivalent one, but decoupling the soft X-ray emission leaking through the partial coverers from the primary emission, which allows us to assign another `polconst` to this component.[4] We set its Π and Ψ to 0 – this is physically motivated by the possibility that the leaked continuum comes from a variety of line-of-sights,

[3] An equivalent fit ($\Delta\chi^2 = +2$ for the same d.o.f.) is obtained by instead deconvolving the reflection components with `rdblur`, which introduce relativistic effects from an accretion disc around a non-rotating black hole (Fabian et al. 1989). As expected, given the modest broadening of the line, the best fit inner radius is very large ($r_{\rm in} = 110^{+40}_{-20}\ r_{\rm g}$, where $r_{\rm g} = GM/c^2$ is the gravitational radius), and the inclination very low ($i = 3^{+5}_{-2}$ deg). All the other parameters are the same, within errors, with respect to those of the best fit.

[4] Each `zpcfabs` has been replaced by the equivalent expression `c*zphabs +(1-c)`, where c is the same covering factor determined in the best fit.

Table 2. Best fit parameters from the spectro-polarimetric analysis.

Parameter	Value
`CLOUDY (Photoionized emitter)`	
$\log U$	1.35 ± 0.01
$\log(N_{\rm H}$ / cm$^{-2})$	21.63 ± 0.02
`PC 1 (Neutral absorber 1)`	
$\log(N_{\rm H}$ /cm$^{-2})$	10.49 ± 0.04
Cf	0.78 ± 0.01
`PC 2 (Neutral absorber 2)`	
$\log(N_{\rm H}$ / cm$^{-2})$	4.36 ± 0.01
Cf	0.95 ± 0.01
`WA (Warm absorber)`	
$\log(N_{\rm H}$ / cm$^{-2})$	$13.60^{+0.92}_{-0.86}$
$\log(\xi$ / erg cm s$^{-1})$	4.12 ± 0.02
`BORUS 1/2 (Neutral reflector 1/2)`	
$\log(N_{\rm H}$ / cm$^{-2})$	24.45 ± 0.01
$A_{\rm Fe}$	0.62 ± 0.01
norm	0.09 ± 0.01
`nthcomp (Comptonized primary continuum)`	
Γ	1.85 ± 0.01
$kT_{\rm e}$ [keV]	60^{+7}_{-6}
norm	0.09 ± 0.01
$\log(F_{2-10\,\rm keV}$ / erg cm^{-2} s$^{-1})$	-9.78 ± 0.01
$\log(L_{2-10\,\rm keV}$ / erg s$^{-1})$	42.61 ± 0.01

or that this further soft component has instead another origin, independent from the primary continuum and not taken into account by our modelling. In this new configuration, with the two polarization angles forced to differ by 90°, the best fit is statistically equivalent to the initial one (χ^2/ d.o.f = 1441/1265), but now all the polarization is attributed to the primary continuum, with $\Pi = 7.7 \pm 1.5\%$ and $\Psi = 87° \pm 6°$, while only an upper limit is found for the reflection component $\Pi < 27\%$. A similar result is obtained if the polarization angles are forced to be the same, but the polarization degree of the reflection component is completely unconstrained in this case.

4 DISCUSSION

4.1 The geometry of the X-ray corona

The measured polarization degree of NGC 4151, determined by both the model-independent and spectro-polarimetric analysis, immediately excludes a 'spherical' lamppost along the disc axis as a possible geometry for the hot corona in this source. Indeed, such a geometry is very symmetric, so the polarization degree is expected to be lower than $1 - 3\%$, even for very high inclinations (e.g. Poutanen & Svensson 1996; Tamborra et al. 2018; Ursini et al. 2022). Moreover, the corresponding polarization angle is expected to be perpendicular to the disc axis, while the measured Ψ is in the direction of the radio emission ($\sim 83°$, Harrison et al. 1986; Ulvestad et al. 1998, and references therein), suggesting instead that the polarization occurs on the equatorial plane. Two other possible coronal geometries are viable and will be considered here: a *slab* extending above and below the accretion disc, and a *wedge*, in which the corona stretches up to the accretion disc with a defined opening angle (Tagliacozzo et al., in prep.). The *slab* geometry is investigated even if it is known to produce relatively soft spectra ($\Gamma \geq 2$) when radiative equilibrium between the disc and the corona is established (e.g. Haardt & Maraschi 1993; Stern et al. 1995 and relevant discussion in Poutanen et al. 2018). The somewhat harder photon index observed in NGC 4151 can still be accommodated with this geometry assuming that the cold accretion disc is truncated at some radius and the inner part is occupied by the hot accretion flow. The seed photons for Comptonization in this case may come from the outer cold disc or be internal synchrotron photons (Veledina et al. 2011). It is very difficult to distinguish between these two scenarios, because in both cases photons undergo many scatterings before they reach the *IXPE* energy band.

We followed the approach of Ursini et al. (2022), performing various simulations with the two geometries, using the general relativistic Monte Carlo radiative transfer code `MONK` (Zhang et al. 2019). We have also cross-checked these results with those obtained with an iterative radiation transport solver (Poutanen & Svensson 1996; Veledina & Poutanen 2022). In our simulations, we assumed a BH mass of $4.57 \times 10^7 M_\odot$ (Bentz et al. 2006), a spin $a = 0.998$ and an Eddington ratio $L_{\rm Bol}/L_{\rm Edd} = 1\%$. As for the corona, we adopted a temperature of 60 keV, as derived from our spectral analysis (see Table 2), and the Thomson optical depth (defined with respect to the half-thickness of the slab/wedge[5]) $\tau = 0.5$, which reproduces the observed photon index ($\Gamma = 1.85$) in both geometries for the given temperature. For both geometries, we consider the inner radius at the innermost stable circular orbit ($R_{\rm in} = 1.24\, r_{\rm g}$), while the outer radius is at $100\, r_{\rm g}$ for the *slab* geometry, and coincides with the inner radius of the accretion disc, $R_{\rm out} = R_{\rm in}^{\rm disc} = 25\, r_{\rm g}$, for the *wedge*. For the latter geometry, the tested opening angles are 30°, 45° and 60°. The height of the slab is $1\, r_{\rm g}$.

It is worth stressing that in all cases, the expected polarization angle is parallel to the disc axis, so in agreement with the observed one. The resulting polarization degree is shown in Figure 3, as a function of the cosine of the inclination angle with respect to the observer. It is clear that the observed polarization degree in NGC 4151 is well reproduced in all cases, only assuming moderate inclinations ($i \gtrsim 40° - 50°$), as reasonable for an intermediate Seyfert galaxy. In particular, the inclination results to be more constrained in the case of the *slab* and for low opening angles of the *wedge*, being in the range $40° - 70°$. On the other hand, for larger opening angles of the *wedge*, the required inclination can be higher. Note that these different geometries also agree with the lack of a significant variation of the polarization degree with energy (e.g., Ursini et al. 2022) in agreement with the observations (see Sect. 3.1 and Table 1).

The disc inclination in NGC 4151 is very uncertain (Marin 2016). It ranges from $i = 0°$ to 33° when estimated via the relativistic reflection component in the X-rays (Nandra et al. 1997; Keck et al. 2015b; Beuchert et al. 2017b; Miller et al. 2018), but a much more inclined system (~58°) is suggested by reverberation studies of the broad-line region (BLR) (Bentz et al. 2022). The mismatch between the various values comes from both the technique and the location of the probed region (the disc or the BLR). Miller et al. (2018) suggested that a warp between the innermost and outer part of the accretion disc in NGC 4151 might resolve this apparent discrepancy in inclination. However, it does not fit the *IXPE* results. In fact, the inclination estimated from BLR reverberation studies matches better the one obtained from the X-ray polarization. A more systematic analysis of bright and nearby Seyfert-1s is needed to verify this conclusion.

[5] This definition is the same as in `compTT` (Titarchuk 1994), while it is half that of `compPS` in the standard configuration (Poutanen & Svensson 1996).

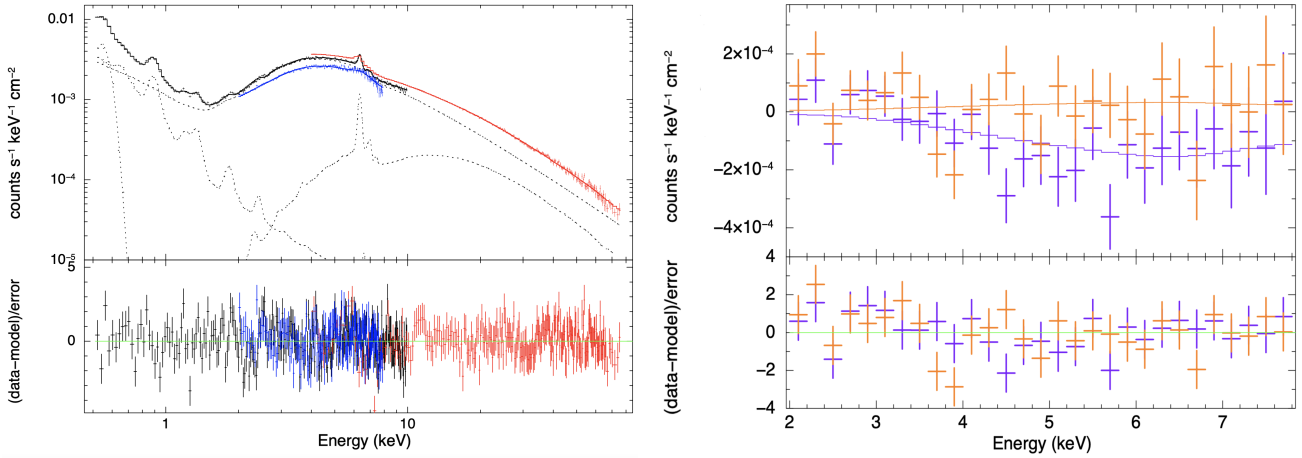

Figure 2. *Left panel: XMM-Newton*/EPIC pn (in black), grouped *NuSTAR* FPMA and FPMB (in red), *IXPE* grouped Stokes I (in blue) simultaneous spectra of NGC 4151 with residuals. The dashed lines represent the different model components. *Right-panel:* Q (in purple) and U (in orange) grouped Stokes spectra are shown with residuals.

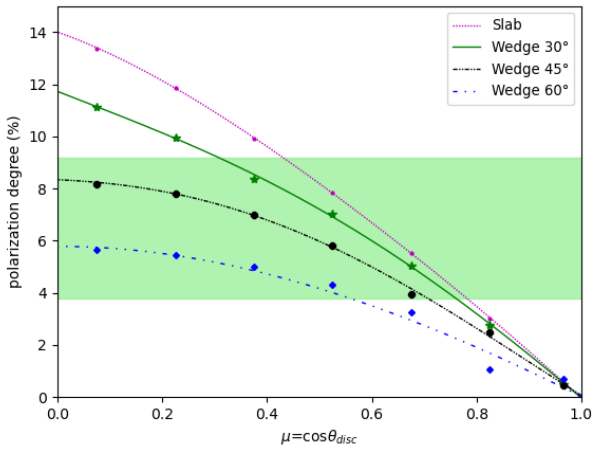

Figure 3. Monte Carlo simulations performed with the Comptonization code MONK. Both *wedge* and *slab* geometry have been considered. The light green band shows the polarization degree range resulting from the model-independent (see Sect. 3.1) and the spectro-polarimetric analysis (see Sect. 3.3). We adopt for all the simulations kT_e = 60 keV and τ = 0.5. The obtained PA is always parallel to the disc axis. See text for details.

4.2 Comparison to lower energies polarization

Marin et al. (2020) presented the most extensive review of the ultraviolet, optical and infrared linear continuum polarization of NGC 4151. From the ultraviolet to the near-infrared ($\lesssim$ 1 μm), the polarization degree is wavelength-dependent but does not exceed 2%, while the polarization position angle remains constant at 80°–90°. Because the polarization angle is parallel to the parsec-scale radio axis, NGC 4151 optical polarization emerges from reprocessing along the equatorial plane. Gaskell et al. (2012) proved, using polarization reverberation mapping, that the polarization emerges from scattering in a flattened region within the low-ionization component of the BLR. The time-lag and polarization angle are inconsistent with both scattering onto the dusty torus and with an intrinsic polarization of the continuum. However, the polarized light spectrum of NGC 4151 appears to corroborate the existence of an optically thick, thermally heated accretion disc structure, at least in its outer near-IR emitting radii (Marin et al. 2020). In the infrared, a smooth rotation of the polarization position angle down to $\sim 45°$ indicates the onset of dichroic absorption from aligned dust grains in the torus. We note that a similar polarization angle is found here in the 2–3.5 keV band ($\psi_X = 42 \pm 11°$, see Table 1), although with lower statistical confidence than at higher energies. Interestingly, this angle would be in agreement with the extended narrow-line region observed with *Chandra* (Wang et al. 2011) and *HST* (45° ± 5°, Evans et al. 1993; Das et al. 2005).

The X-ray polarization degree we measured is different from the archival and contemporaneous[6] ultraviolet, optical and infrared polarization of NGC 4151. It indicates that X-ray polarization comes from a different region than the BLR or the torus, and is indeed consistent with an origin in a slab-like corona. The polarization angle, however, is the same as in the ultraviolet and optical, indicating that reprocessing mainly occurs along the equatorial plane from the X-rays to the near-infrared. A deeper analysis of the X-ray to infrared polarization of NGC 4151 will be presented in a future paper.

ACKNOWLEDGEMENTS

The Imaging X-ray Polarimetry Explorer (*IXPE*) is a joint US and Italian mission. The US contribution is supported by the National Aeronautics and Space Administration (NASA) and led and managed by its Marshall Space Flight Center (MSFC), with industry partner Ball Aerospace (contract NNM15AA18C). The Italian contribution is supported by the Italian Space Agency (Agenzia Spaziale Italiana, ASI) through contract ASI-OHBI-2017-12-I.0, agreements ASI-INAF-2017-12-H0 and ASI-INFN-2017.13-H0, and its Space Science Data Center (SSDC) with agreements ASI- INAF-2022-14-HH.0 and ASI-INFN 2021-43-HH.0, and by the Istituto Nazionale di Astrofisica (INAF) and the Istituto Nazionale di Fisica Nucleare (INFN) in Italy. This research used data products provided by the *IXPE* Team (MSFC, SSDC, INAF, and INFN) and distributed with

[6] B, V, R and I broadband polarimetry of NGC 4151 was obtained contemporaneously to the *IXPE* observation using the Perkins Telescope observatory. Those new measurements are in all respects similar to the archival data and will be presented in a future publication compiling recent optical polarimetric data from Changing Look AGNs.

additional software tools by the High-Energy Astrophysics Science Archive Research Center (HEASARC), at NASA Goddard Space Flight Center (GSFC). We thank the *XMM-Newton* and *NuSTAR* SOCs for granting and performing the respective observations of the source. Part of the French contribution is supported by the Scientific Research National Center (CNRS) and the French Space Agency (CNES).

DATA AVAILABILITY

The *IXPE* data used in this paper are publicly available in the HEASARC database (https://heasarc.gsfc.nasa.gov/docs/ixpe/archive/). The *XMM-Newton* and *NuSTAR* data underlying this article are subject to an embargo of 12 months from the date of the observations. Once the embargo expires the data will be publicly available from the *XMM-Newton* science archive (http://nxsa.esac.esa.int/) and the *NuSTAR* archive (https://heasarc.gsfc.nasa.gov/docs/nustar/nustar_archive.html). The MONK simulation data supporting the findings of the article will be shared on reasonable request.

REFERENCES

Anders E., Grevesse N., 1989, Geochimica Cosmochimica Acta, 53, 197
Antonucci R., 1993, ARA&A, 31, 473
Antonucci R. R. J., Cohen R. D., 1983, ApJ, 271, 564
Arnaud K. A., 1996, in Jacoby G. H., Barnes J., eds, ASP Conf. Ser. Vol. 101, Astronomical Data Analysis Software and Systems V. Astron. Soc. Pac., San Francisco, pp 17–20
Baldini L., et al., 2021, Astroparticle Physics, 133, 102628
Baldini L., et al., 2022, SoftwareX, 19, 101194
Baloković M., et al., 2018, ApJ, 854, 42
Baloković M., García J. A., Cabral S. E., 2019, Research Notes of the American Astronomical Society, 3, 173
Bellazzini R., et al., 2003, in Fineschi S., ed., Vol. 4843, Polarimetry in Astronomy. SPIE, pp 372–382, doi:10.1117/12.459380, https://doi.org/10.1117/12.459380
Bellazzini R., et al., 2007, Nuclear Instruments and Methods in Physics Research A, 579, 853
Bentz M. C., et al., 2006, ApJ, 651, 775
Bentz M. C., Williams P. R., Treu T., 2022, ApJ, 934, 168
Beuchert T., et al., 2017a, A&A, 603, A50
Beuchert T., et al., 2017b, A&A, 603, A50
Bianchi S., Guainazzi M., Chiaberge M., 2006, A&A, 448, 499
Bianchi S., Chiaberge M., Evans D. A., Guainazzi M., Baldi R. D., Matt G., Piconcelli E., 2010, MNRAS, 405, 553
Bianchi S., Guainazzi M., Laor A., Stern J., Behar E., 2019, MNRAS, 485, 416
Brightman M., et al., 2015, ApJ, 805, 41
Cackett E. M., Zoghbi A., Reynolds C., Fabian A. C., Kara E., Uttley P., Wilkins D. R., 2014, MNRAS, 438, 2980
Costa E., Soffitta P., Bellazzini R., Brez A., Lumb N., Spandre G., 2001, Nature, 411, 662
Das V., et al., 2005, AJ, 130, 945
De Rosa A., Piro L., Perola G. C., Capalbi M., Cappi M., Grandi P., Maraschi L., Petrucci P. O., 2007, A&A, 463, 903
Di Gesu L., et al., 2022, ApJ, 938, L7
Di Marco A., et al., 2022, AJ, 163, 170
Di Marco A., et al., 2023, AJ, 165, 143
Evans I. N., Tsvetanov Z., Kriss G. A., Ford H. C., Caganoff S., Koratkar A. P., 1993, ApJ, 417, 82
Fabian A. C., Rees M. J., Stella L., White N. E., 1989, MNRAS, 238, 729
Fabian A. C., Lohfink A., Belmont R., Malzac J., Coppi P., 2017, MNRAS, 467, 2566
Fabiani S., Muleri F., 2014, Astronomical X-Ray Polarimetry. Astronomia e astrofisica, Aracne, https://books.google.it/books?id=K_MFogEACAAJ
Fabiani S., et al., 2012, Advances in Space Research, 49, 143
Ferland G. J., Korista K. T., Verner D. A., Ferguson J. W., Kingdon J. B., Verner E. M., 1998, PASP, 110, 761
Ferrazzoli R., et al., 2020, J. Astron. Telesc. Instrum. Syst., 6, 048002
Gaskell C. M., Goosmann R. W., Merkulova N. I., Shakhovskoy N. M., Shoji M., 2012, ApJ, 749, 148
Ghisellini G., Haardt F., Matt G., 2004, A&A, 413, 535
Guainazzi M., Bianchi S., 2007, MNRAS, 374, 1290
Haardt F., Maraschi L., 1991, ApJ, 380, L51
Haardt F., Maraschi L., 1993, ApJ, 413, 507
Harrison B., Pedlar A., Unger S. W., Burgess P., Graham D. A., Preuss E., 1986, MNRAS, 218, 775
Harrison F. A., et al., 2013, ApJ, 770, 103
Kalberla P. M. W., Burton W. B., Hartmann D., Arnal E. M., Bajaja E., Morras R., Pöppel W. G. L., 2005, A&A, 440, 775
Keck M. L., et al., 2015a, ApJ, 806, 149
Keck M. L., et al., 2015b, ApJ, 806, 149
Kislat F., Clark B., Beilicke M., Krawczynski H., 2015, Astroparticle Physics, 68, 45
Kraemer S. B., Schmitt H. R., Crenshaw D. M., 2008, ApJ, 679, 1128
LaMassa S. M., Yaqoob T., Boorman P. G., Tzanavaris P., Levenson N. A., Gandhi P., Ptak A. F., Heckman T. M., 2019, ApJ, 887, 173
Lubiński P., Zdziarski A. A., Walter R., Paltani S., Beckmann V., Soldi S., Ferrigno C., Courvoisier T. J. L., 2010, MNRAS, 408, 1851
Madsen K. K., Grefenstette B. W., Pike S., Miyasaka H., Brightman M., Forster K., Harrison F. A., 2020, arXiv e-prints, p. arXiv:2005.00569
Marin F., 2016, MNRAS, 460, 3679
Marin F., Le Cam J., Lopez-Rodriguez E., Kolehmainen M., Babler B. L., Meade M. R., 2020, MNRAS, 496, 215
Marinucci A., et al., 2022, MNRAS, 516, 5907
Merloni A., 2003, MNRAS, 341, 1051
Miller J. M., et al., 2018, ApJ, 865, 97
Nandra K., George I. M., Mushotzky R. F., Turner T. J., Yaqoob T., 1997, ApJ, 476, 70
Penston M. V., Perez E., 1984, MNRAS, 211, 33P
Poutanen J., Svensson R., 1996, ApJ, 470, 249
Poutanen J., Veledina A., Zdziarski A. A., 2018, A&A, 614, A79
Puccetti S., Fiore F., Risaliti G., Capalbi M., Elvis M., Nicastro F., 2007, MNRAS, 377, 607
Rankin J., et al., 2022, AJ, 163, 39
Schurch N. J., Warwick R. S., Griffiths R. E., Kahn S. M., 2004, MNRAS, 350, 1
Shakura N. I., Sunyaev R. A., 1973, A&A, 24, 337
Shapiro S. L., Lightman A. P., Eardley D. M., 1976, ApJ, 204, 187
Shapovalova A. I., et al., 2008, A&A, 486, 99
Shapovalova A. I., et al., 2012, Astron. Astrophys. Trans., 27, 429
Stern B. E., Poutanen J., Svensson R., Sikora M., Begelman M. C., 1995, ApJ, 449, L13
Strüder L., et al., 2001, A&A, 365, L18
Sunyaev R. A., Titarchuk L. G., 1980, A&A, 86, 121
Szanecki M., Niedźwiecki A., Zdziarski A. A., 2021, ApJ, 909, 205
Tamborra F., Matt G., Bianchi S., Dovčiak M., 2018, A&A, 619, A105
Titarchuk L., 1994, ApJ, 434, 570
Turner M. J. L., et al., 2001, A&A, 365, L27
Ulvestad J. S., Roy A. L., Colbert E. J. M., Wilson A. S., 1998, ApJ, 496, 196
Ursini F., Matt G., Bianchi S., Marinucci A., Dovčiak M., Zhang W., 2022, MNRAS, 510, 3674
Ursini F., et al., 2023, MNRAS, 519, 50
Veledina A., Poutanen J., 2022, Polarization of Comptonized emission in slab geometry, doi:10.5281/zenodo.7116125, https://doi.org/10.5281/zenodo.7116125
Veledina A., Vurm I., Poutanen J., 2011, MNRAS, 414, 3330
Wang J., et al., 2011, ApJ, 742, 23

Weaver K. A., et al., 1994, ApJ, 423, 621
Weisskopf M. C., et al., 2022, J. Astron. Telesc. Instrum. Syst., 8, 026002
Wolfinger K., Kilborn V. A., Koribalski B. S., Minchin R. F., Boyce P. J., Disney M. J., Lang R. H., Jordan C. A., 2013, MNRAS, 428, 1790
Yang Y., Wilson A. S., Ferruit P., 2001, ApJ, 563, 124
Zdziarski A. A., Johnson W. N., Magdziarz P., 1996, MNRAS, 283, 193
Zdziarski A. A., Poutanen J., Johnson W. N., 2000, ApJ, 542, 703
Zhang W., Dovčiak M., Bursa M., 2019, ApJ, 875, 148
Zoghbi A., Miller J. M., Cackett E., 2019, ApJ, 884, 26
Życki P. T., Done C., Smith D. A., 1999, MNRAS, 309, 561

Affiliations:
[1]*Université Grenoble Alpes, CNRS, IPAG, 38000 Grenoble, France*
[2]*Dipartimento di Matematica e Fisica, Università degli Studi Roma Tre, Via della Vasca Navale 84, 00146 Roma, Italy*
[3]*INAF Istituto di Astrofisica e Planetologia Spaziali, Via del Fosso del Cavaliere 100, I-00133 Roma, Italy*
[4]*Dipartimento di Fisica, Università degli Studi di Roma "La Sapienza", Piazzale Aldo Moro 5, I-00185 Roma, Italy*
[5]*Dipartimento di Fisica, Università degli Studi di Roma "Tor Vergata", Via della Ricerca Scientifica 1, I-00133 Roma, Italy*
[6]*Instituto de Astrofísica de Andalucía—CSIC, Glorieta de la Astronomía s/n, 18008 Granada, Spain*
[7]*Department of Physics and Kavli Institute for Particle Astrophysics and Cosmology, Stanford University, Stanford, California 94305, USA*
[8]*Université de Strasbourg, CNRS, Observatoire Astronomique de Strasbourg, UMR 7550, 67000 Strasbourg, France*
[9]*ASI - Agenzia Spaziale Italiana, Via del Politecnico snc, 00133 Roma, Italy*
[10]*Space Science Data Center, Agenzia Spaziale Italiana, Via del Politecnico snc, 00133 Roma, Italy*
[11]*Istituto Nazionale di Fisica Nucleare, Sezione di Roma "Tor Vergata", Via della Ricerca Scientifica 1, 00133 Roma, Italy*
[12]*Department of Astronomy, University of Maryland, College Park, Maryland 20742, USA*
[13]*School of Mathematics, Statistics, and Physics, Newcastle University, Newcastle upon Tyne NE1 7RU, UK*
[14]*Department of Physics and Astronomy, 20014 University of Turku, Finland*
[15]*MIT Kavli Institute for Astrophysics and Space Research, Massachusetts Institute of Technology, 77 Massachusetts Avenue, Cambridge, MA 02139, USA*
[16]*Astronomical Institute of the Czech Academy of Sciences, Boční II 1401/1, 14100 Praha 4, Czech Republic*
[17]*Astronomical Institute, Charles University, V Holešovičkách 2, CZ-18000 Prague, Czech Republic*
[18]*Nordita, KTH Royal Institute of Technology and Stockholm University, Hannes Alfvéns väg 12, SE-10691 Stockholm, Sweden*
[19]*National Astronomical Observatories, Chinese Academy of Sciences, 20A Datun Road, Beijing 100101, China*
[20]*INAF Osservatorio Astronomico di Roma, Via Frascati 33, 00078 Monte Porzio Catone (RM), Italy*
[21]*INAF Osservatorio Astronomico di Cagliari, Via della Scienza 5, 09047 Selargius (CA), Italy*
[22]*Istituto Nazionale di Fisica Nucleare, Sezione di Pisa, Largo B. Pontecorvo 3, 56127 Pisa, Italy*
[23]*Dipartimento di Fisica, Università di Pisa, Largo B. Pontecorvo 3, 56127 Pisa, Italy*
[24]*NASA Marshall Space Flight Center, Huntsville, AL 35812, USA*
[25]*Istituto Nazionale di Fisica Nucleare, Sezione di Torino, Via Pietro Giuria 1, 10125 Torino, Italy*
[26]*Dipartimento di Fisica, Università degli Studi di Torino, Via Pietro Giuria 1, 10125 Torino, Italy*
[27]*INAF Osservatorio Astrofisico di Arcetri, Largo Enrico Fermi 5, 50125 Firenze, Italy*
[28]*Dipartimento di Fisica e Astronomia, Università degli Studi di Firenze, Via Sansone 1, 50019 Sesto Fiorentino (FI), Italy*
[29]*Istituto Nazionale di Fisica Nucleare, Sezione di Firenze, Via Sansone 1, 50019 Sesto Fiorentino (FI), Italy*
[30]*Science and Technology Institute, Universities Space Research Association, Huntsville, AL 35805, USA*
[31]*Institut für Astronomie und Astrophysik, Universität Tübingen, Sand 1, 72076 Tübingen, Germany*
[32] *RIKEN Cluster for Pioneering Research, 2-1 Hirosawa, Wako, Saitama 351-0198, Japan*
[33]*California Institute of Technology, Pasadena, CA 91125, USA*
[34]*Yamagata University, 1-4-12 Kojirakawamachi, Yamagatashi 990-8560, Japan*
[35]*University of British Columbia, Vancouver, BC V6T 1Z4, Canada*
[36]*International Center for Hadron Astrophysics, Chiba University, Chiba 263-8522, Japan*
[37]*Institute for Astrophysical Research, Boston University, 725 Commonwealth Avenue, Boston, MA 02215, USA*
[38]*Department of Astrophysics, St. Petersburg State University, Universitetsky pr. 28, Petrodvoretz, 198504 St. Petersburg, Russia*
[39]*Department of Physics and Astronomy and Space Science Center, University of New Hampshire, Durham, NH 03824, USA*
[40]*Physics Department and McDonnell Center for the Space Sciences, Washington University in St. Louis, St. Louis, MO 63130, USA*
[41]*Finnish Centre for Astronomy with ESO, 20014 University of Turku, Finland*
[42]*Graduate School of Science, Division of Particle and Astrophysical Science, Nagoya University, Furocho, Chikusaku, Nagoya, Aichi 464-8602, Japan*
[43]*Hiroshima Astrophysical Science Center, Hiroshima University, 1- 3-1 Kagamiyama, Higashi-Hiroshima, Hiroshima 739-8526, Japan*
[44]*University of Maryland, Baltimore County, Baltimore, MD 21250, USA*
[45]*NASA Goddard Space Flight Center, Greenbelt, MD 20771, USA*
[46]*Center for Research and Exploration in Space Science and Technology, NASA/GSFC, Greenbelt, MD 20771, USA*
[47]*Department of Physics, The University of Hong Kong, Pokfulam, Hong Kong*
[48]*Department of Astronomy and Astrophysics, Pennsylvania State University, University Park, PA 16802, USA*
[49]*Center for Astrophysics | Harvard & Smithsonian, 60 Garden St, Cambridge, MA 02138, USA*
[50]*INAF Osservatorio Astronomico di Brera, Via E. Bianchi 46, 23807 Merate (LC), Italy*
[51]*Dipartimento di Fisica e Astronomia, Università degli Studi di Padova, Via Marzolo 8, 35131 Padova, Italy*
[52]*Mullard Space Science Laboratory, University College London, Holmbury St Mary, Dorking, Surrey RH5 6NT, UK*
[53]*Anton Pannekoek Institute for Astronomy & GRAPPA, University of Amsterdam, Science Park 904, 1098 XH Amsterdam, The Netherlands*
[54]*Guangxi Key Laboratory for Relativistic Astrophysics, School of Physical Science and Technology, Guangxi University, Nanning 530004, China*

This paper has been typeset from a TEX/LATEX file prepared by the author.